Correlations of Inhibitor Kinetics for *Pneumocystis jirovecii* and Human Dihydrofolate Reductase with Structural Data for Human Active Site Mutant Enzyme Complexes[†,‡]

Vivian Cody,[*,§,||] Jim Pace,[§] Jennifer Makin,[§] Jennifer Piraino,[§] Sherry F. Queener,[⊥] and Andre Rosowsky[#]

Structural Biology Department, Hauptman−Woodward Medical Research Institute, 700 Ellicott Street, Buffalo, New York 14203, Structural Biology Department, School of Medicine and Biological Sciences, State University of New York at Buffalo, Buffalo, New York 14260, Department of Pharmacology and Toxicology, Indiana University School of Medicine, Indianapolis, Indiana 46202, and Dana-Farber Cancer Institute, Harvard Medical School, Boston, Massachusetts 02115

Received October 20, 2008; Revised Manuscript Received January 9, 2009

ABSTRACT: To understand the role of specific active site residues in conferring selective dihydrofolate reductase (DHFR) inhibition from pathogenic organisms such as *Pneumocystis carinii* (pc) or *Pneumocystis jirovecii* (pj), the causative agent in AIDS pneumonia, it is necessary to evaluate the role of these residues in the human enzyme. We report the first kinetic parameters for DHFR from pjDHFR and pcDHFR with methotrexate (MTX), trimethoprim (TMP), and its potent analogue, PY957. We also report the mutagenesis and kinetic analysis of active site mutant proteins at positions 35 and 64 of human (h) DHFR and the crystal structure determinations of hDHFR ternary complexes of NADPH and PY957 with the wild-type DHFR enzyme, the single mutant protein, Gln35Lys, and two double mutant proteins, Gln35Ser/Asn64Ser and Gln35Ser/Asn64Phe. These substitutions place into human DHFR amino acids found at those sites in the opportunistic pathogens pcDHFR (Q35K/N64F) and pjDHFR (Q35S/N64S). The K_i inhibition constant for PY957 showed greatest potency of the compound for the N64F single mutant protein (5.2 nM), followed by wild-type pcDHFR (K_i 22 nM) and then wild-type hDHFR enzyme (K_i 230 nM). Structural data reveal significant conformational changes in the binding interactions of PY957 in the hDHFR Q35S/N64F mutant protein complex compared to the other hDHFR mutant protein complexes and the pcDHFR ternary complex. The conformation of PY957 in the wild-type DHFR is similar to that observed for the single mutant protein. These data support the hypothesis that the enhanced selectivity of PY957 for pcDHFR is in part due to the contributions at positions 37 and 69 (pcDHFR numbering). This insight will help in the design of more selective inhibitors that target these opportunistic pathogens.

The atypical fungus *Pneumocystis jirovecii* (pj)[1] is an opportunistic pathogen that causes life-threatening *Pneumocystis* pneumonia (PcP), one of the most prevalent opportunistic infections in patients with HIV AIDS (*1*−*3*). Current treatment of PcP combines the sulfa drug sulfamethoxazole with trimethoprim (TMP) (Figure 1) that targets folate biosynthesis (*1, 4*). Initial characterization of pjDHFR derived from patients with HIV AIDS (*5*) showed that it was similar to *Pneumocystis carinii* (pcDHFR) found in rat lungs but showed significant sequence differences (Table 1). These data also showed that TMP was a weak competitive inhibitor with a K_i value of 2.8×10^{-7} M. In contrast, MTX was a tight-binding competitive inhibitor with a K_i of 1.6×10^{-11} M (*5*).

Recent studies have also shown the emergence of TMP drug resistance related to mutations in DHFR. For example, in a study of patients with PcP, some treated with a DHFR inhibitor and some with no prophylaxis, 19 DHFR nucleotide substitution sites were observed in 18 patients, with 16 of these sites giving rise to mutations (*6*). These data suggest that different *P. jirovecii* populations with alternate forms of the target enzyme may arise with selective pressure from DHFR inhibitors.

Since *P. jirovecii* cannot be grown in culture and will not reproduce in experimental animals, most drug design efforts have targeted DHFR from *P. carinii* found in rat lungs (*7*−*10*). Although these two forms of DHFR are similar, they differ in their drug sensitivity. These differences provide an opportunity to design selective drugs that target a specific

[†] This work was supported in part by a grant from the National Institutes of Health (GM51670 to V.C.).

[‡] Coordinates and crystallographic structure factors for human DHFR mutant complexes have been deposited in the Protein Data Bank under the accession codes 3F8Y, 3F87, 3F91, and 3FS6.

* To whom correspondence should be addressed. E-mail: cody@hwi.buffalo.edu. Phone: 716-898-8614. Fax: 716-898-8660.

[§] Hauptman Woodward Medical Research Institute.

[||] State University of New York at Buffalo.

[⊥] Indiana University School of Medicine.

[#] Harvard Medical School.

[1] Abbreviations: DHFR, dihydrofolate reductase; DHFA, dihydrofolic acid; pj, *Pneumocystis jirovecci*; pc, *Pneumocystis carinii*; IC_{50}, concentration giving 50% inhibition; K_i, inhibition constant for inhibition.

[2] The numbering used throughout this paper for the human DHFR sequence is based on the first position being Val-1 rather than Met-1 as observed in the gene sequence listing. This numbering has been used in previous publications of the kinetic and structural data for hDHFR and is being used here for continuity.

10.1021/bi801960h CCC: $40.75
Published on Web 02/05/2009

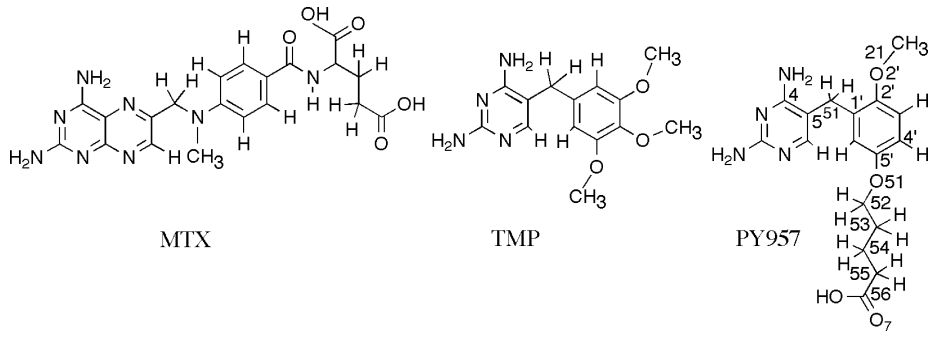

FIGURE 1: Schematic representation of antifolates under study.

Table 1: Sequence Alignment of Human (h) (186 Residues), *P. carinii* (pc), and *P. jirovecii* (pj) (Both 206 Residues) DHFR[a]

```
                                                  30 31   35  38 39
hDHFR   --MVGSLNCIVAVSQNMGIGKNGDLPWPPLRNEFRYFQRMTT---TSSVEGKQNLVIMGK

pcDHFR MNQQKSLTLIVALTTSYGIGRSNSLPWK-LKKEISYFKRVTSFVPTFDSFESMNVVLMGR

pjDHFR MDWQKSLTLIVALTLSRGIGLKNDLPWK-LKSDMMFFSRVTSGLLVTRSTGQMNVVLMGR

           59 60 64    70
hDHFR   KTWFSIPEKNRPLKGRINLVLSRELKEPPQGAHFLSRSLDDALKLTEQ---PELANKVDM

pcDHFR KTWESIPLQFRPLKGRINVVITRNESLDLGNGIHSAKSLDHALELLYRTYGSESSVQINR

pjDHFR KTWESLPAHSRPLKNRINVVISRQEVLDLGGGAYHARSLDDALALLSQIYDSTSKIQLNR


hDHFR   VWIVGGSSVYKEAMNHPGHLKLFVTRIMQDFESDTFFPEIDLEKYKLLPEYPGVLSDVQ-

pcDHFR IFVIGGAQLYKAAMDHPKLDRIMATIIYKDIHCDVFFPLKFRDKEWSSVWKKEKHSDLES

pjDHFR VFVIGGGELYKAAMEHSRLNRIIATVIHNEVDCDVFFPIDFRSSQSCLPWRKQDHSVLEA

                                    186
hDHFR   -----------EEKGIKYKFEVYEKND

pcDHFR WVGTKVPHGKINEDGFDYEFEMWTRDL

pjDHFR WVGSKVPQGKINENGFIYEFEMWIRDI
```

[a] Mutational sites are underlined and in red while key active site residues are numbered and colored cyan [CLUSTAL FORMAT for T-COFFEE Version_5.68 (http://www.tcoffee.org)].

species of enzyme. This will of necessity require careful consideration of crucial differences in the active sites among these two fungal enzymes and human DHFR. Of note is the variability observed among the human and fungal enzyme sequences in the active site, in particular residues at positions 35 and 64 (hDHFR numbering, Table 1).[2] In the human enzyme these residues are Gln and Asn, while in pcDHFR they are Lys and Phe, and Ser and Ser in pjDHFR. Structural data for inhibitor binding to h- or pcDHFR reveals that these residues interact with antifolates (*11*) and that inhibitors can be designed to target interactions with these residues (*9*−*11*).

In order to assess the role of active site variants among the pathogenic DHFR enzymes, whether as single or double mutant proteins, it is important to understand the role of these residues in giving rise to TMP resistance by weaker binding or in giving rise to enhanced native-like activity (*12, 13*). In a study to screen for MTX resistance of hDHFR, synergistic resistance could be obtained by combining two or more active site mutations that confer weak MTX resistance (*12*). In the combinatorial libraries that were created for positions 31, 34, and 35, mutations of Gln35 were observed that reflected the residues for pc- and pjDHFR (i.e., Q35K, Q35S). Neither of these mutations caused MTX resistance. Recent studies have also suggested that the effect of double mutants in an active site may be additive, partially additive, synergistic, antagonistic, or absent (*14*).

Efforts to produce more selective and potent antifolates that target pcDHFR led to the design of novel 2,4-diamino-5-(ω-carboxyalky)oxy trimethoprim analogue that showed 80−5000-fold increase in potency (IC_{50}) over the mammalian enzyme (*15*). We used PY957 (Figure 1), a potent and selective compound from this series, to explore the critical differences in the active sites of mammalian and *Pneumocystis* DHFR. Herein we report the first kinetic analysis of recombinant pjDHFR, pcDHFR, and hDHFR and for a larger series of active site mutants of hDHFR designed to explore sequence differences between the human and the two *Pneumocystis* enzymes (Tables 1, 2, and 3), and the potent inhibitors, methotrexate (MTX), trimethoprim (TMP), and its analogue, PY957. Additionally, we report the crystal structures of human DHFR bearing the single amino acid substitution (Q35K) and hDHFR bearing two double sub-

Table 2: Kinetic Constants for Substrate and Cofactor for pj-, pc-, and hDHFR and Its Active Site Mutants That Reflect Human to *Pneumocystis* Changes

enzyme	K_m(DHFA) (μM)	K_m(NADPH) (μM)	k_{cat} (s^{-1})	k_{cat}/K_m(DHFA) (s^{-1} μM)
pjDHFR	2.8 ± 0.04 (n = 2)	22.9 ± 2.1[a] (n = 2)	53 ± 4.2 (n = 6)	19
pcDHFR	4.9 ± 0.3[a] (n = 5)	14.5 ± 2.2 (n = 2)	284 ± 13[a] (n = 3)	58
pcDHFR K37Q	8.5 ± 0.87 (n = 7)	9.2 ± 1.9 (n = 1)	36 ± 2.4 (n = 9)	4
hDHFR	2.7 ± 0.5 (n = 4)	4.0 ± 1.8 (n = 2)	40 ± 2.2 (n = 8)	15
Mutants h → pjDHFR				
Q35S	1.1 ± 0.4 (n = 4)	4.4 ± 2.0 (n = 2)	35 ± 3.3 (n = 4)	33
N64S	0.18 ± 0.06 (n = 2)	6.3 ± 0.5 (n = 1)	47 ± 5.3 (n = 3)	261
Q35S/N64S	1.6 ± 0.4 (n = 2)	4.6 ± 2.2 (n = 2)	27 ± 4.5 (n = 2)	17
Mutants h → pcDHFR				
Q35K	0.76 ± 0.2[a] (n = 4)	13.0 ± 0.5 (n = 2)	48 ± 4.0 (n = 6)	63
N64F	0.81 ± 0.3[a] (n = 3)	5.2 ± 2.8 (n = 2)	40 ± 7.5 (n = 3)	49
Q35K/N64F	0.49 ± 0.05[a] (n = 4)	5.5 ± 1.8 (n = 2)	43 ± 2.5 (n = 4)	88

[a] Value is statistically different from the value for native human DHFR.

Table 3: Kinetic Constants for Selected Antifolates against pjDHFR, pcDHFR, and Wild-Type and Mutant hDHFR

	K_i (nM)		
enzyme	TMP	MTX	PY957
pjDHFR	43 ± 5[a] (n = 14)	0.042 ± 0.010 (n = 13)	26.3 ± 7.4[a] (n = 7)
pjDHFR (*5*)	28 ± 2 (n = 2)	0.062 ± 0.013 (n = 2)	
pcDHFR	800 ± 300[a] (n = 7)	0.014 ± 0.004[a] (n = 4)	21.9 ± 9.3[a] (n = 7)
pcDHFR K37Q	75.0 ± 3.9 (n = 5)	0.063 ± 0.4 (n = 6)	7.6 ± 1.9 (n = 6)
hDHFR	5200 ± 700 (n = 4)	0.093 ± 0.021 (n = 8)	230 ± 20 (n = 4)
Mutant h → pjDHFR			
hDHFR Q35S	1800 ± 100[a] (n = 3)	0.047 ± 0.008 (n = 3)	350 ± 130 (n = 3)
hDHFR N64S	170 ± 0.5[a] (n = 2)	0.003 ± 0.004[a] (n = 2)	23 ± 14[a] (n = 2)
hDHFR Q35S/N64S	1200 ± 100[a] (n = 4)	0.047 ± 0.007 (n = 4)	66 ± 2[a] (n = 3)
Mutant h → pcDHFR			
hDHFR Q35K	390 ± 30[a] (n = 2)	0.002 ± 0.0002[a] (n = 2)	8.3 ± 0.4[a] (n = 4)
hDHFR N64F	490 ± 160[a] (n = 3)	0.029 ± 0.006[a] (n = 3)	5.2 ± 1.6[a] (n = 2)
hDHFR Q35K/N64F	650 ± 180[a] (n = 5)	0.019 ± 0.006[a] (n = 8)	13 ± 3[a] (n = 2)

[a] Value is statistically different from the value for native human DHFR.

stitutions (Q35S/N64S and Q35S/N64F), as ternary complexes with NADPH and PY957. The crystal structure of PY957 with wild-type pcDHFR has been reported (*16*). Taken together, these data enrich our understanding of the role of DHFR active site residues in conferring species selectivity and specificity of antifolate binding.

EXPERIMENTAL PROCEDURES

Expression and Purification of pj- and pcDHFR. The cDNA for pj- or pcDHFR was transfected into *Escherichia coli* Rosetta Gami B (DE3) competent cells with pET-SUMO-DHFR plasmid for expression. The general expression protocol is to inoculate a 10 mL culture of Luria broth (LB) containing ampicillin (AMP), grown overnight at 37 °C, inoculate 1 L of LB containing antibiotic, and grow at 37 °C to an OD_{600} of 0.6−0.8. The cells are then induced with isopropyl β-D-thiogalactopyranoside (IPTG) at a final concentration of 1 mM, shaken overnight at 16 °C, and harvested by centrifugation at 4 °C at 12000*g*. The cell pellets were resuspended in a lysis buffer (100 mL of ice-cold buffer containing 6.8 g of KH_2PO_4 and 3.7 g of KCl dissolved in 900 mL of H_2O, and 1.0 M ethylenediaminetetraacetic acid (EDTA), and adjusted to pH 7.0 with KOH before bringing the volume to 1 L) and the cells broken using a microfluidizer at 18000 psi (Microfluidics, Inc.). The SUMO fusion protein has the His tag for Ni-column purification. The tag is removed by the SUMO protease (*17*), leaving a native protein. A two-step purification protocol using a Ni-chelating IMAC for removal of the His-tagged protein, followed by Ulp1 protease cleavage, and passage over a second IMAC column resulted in a yield of 20−30 mg of purified enzyme from 1 L of culture.

Construction and Expression of Mutant Human DHFR. Mutations were introduced into the cDNA of hDHFR, and the entire coding sequence was verified by Roswell Park Cancer Center (Buffalo, NY). DNA oligonucleotides were obtained from Integrated DNA Technologies (Coralville, IA) and used without further purification. Plasmid DNA was purified using the plasmid mini kit (Qiagen). Mutagenesis was performed using the QuikChange site-directed mutagenesis kit (Stratagene). All primers were PAGE purified and were synthesized by Alpha DNA (Montreal, Quebec) or IDT (Coralville, IA). Primers were designed according to manufacturer's recommendations as were the PCR reactions, with adjustments made for the T_m of the respective primer. PCR (50 ng of dsDNA template, 100 ng of each primer, 5 mM dNTPs, 2.5 units/μL Taq): 1 cycle of 95 °C for 30 s, 16 cycles of 95 °C for 30 s, 55 °C for 1 min, and 68 °C for 3 min. Primers (5′ to 3′): Q35K for, CAGATATTTCAAGAGAATGACCACAACC; Q35K rev, GGTTGTGGTCATTCTCTTGAAATATCTG; Q35S for, CAGATATTTCTCGAGAATGACCACAACC; Q35S rev, GGTTGTGGTCATTCTCGAGAAATATCTG; N64F for, GGTTCTCCATTCCTGAGAAGTTTCGACCTTTAAAGGGTAG; N64F rev, CTACCCTTTAAAGGTCGAAACTTCTCAGGAATGGAGAACC; N64S for, GGTTCTCCATTCCTGAGAAGAGTCGACCTTTAAAGGGTAG; N64S rev, CTACCCTTTAAAGGTCGACTCTTCTCAGGAATGGAGAACC.

The original wild-type human DHFR (pDS5 vector) was used for PCR and all subsequent mutagenesis experiments. Four single mutants were created (Q35K, Q35S, N64F, and N64S) with the QuikChange site-directed mutagenesis kit following the manufacturer's recommended conditions. Four double mutant proteins (Q35K/N64F, Q35S/N64F, Q35K/N64S, Q35S/N64S) were created by using parental template DNA having one confirmed single residue mutation and using primers for the second desired mutation during PCR.

Expression and Purification of Human DHFR pDS5/Mutant pDS5. The following protocol was used for expression of wild-type (wt) human DHFR (*18*) and mutant human DHFR in the pDS5 vector in *E. coli* BL21(DE3): 200 mL of LB medium containing 100 μg/mL AMP was inoculated with glycerol stock of hDHFR at 37 °C with shaking at 300 rpm overnight. One liter of fresh LB/AMP was inoculated with the 200 mL culture overnight and grown at 37 °C at 300 rpm until the OD_{600} reached 0.8−0.9. Cells were then induced with 2 mM IPTG overnight at 16 °C (16−18 h) and harvested by centrifugation at 13000*g*. Cells were resuspended in 100 mL of ice-cold M9 salt solution (12.8 g of $Na_2HPO_4 \cdot 7H_20$, 3 g of KH_2PO_4, 0.5 g of NaCl, 1 g of NH_4Cl in a volume of 1 L).

Cells were lysed in 100 mL of ice-cold buffer containing 6.8 g of KH_2PO_4, 3.7 g of KCl, dissolved in 900 mL of H_2O, 1.0 mL of 1.0 M ethylenediaminetetraacetic acid (EDTA) was added, and the pH was adjusted to 7.0 with KOH before bringing the volume to 1 L. Cells were disrupted by passing through a microfluidizer at 18000 psi (Microfluidics, Inc.). The resulting lysate was subjected to centrifugation for 30 min at 7000*g*. Ammonium sulfate was added to supernatant over a period of 60 min to a final saturation of 85% at 0 °C. Precipitated protein was centrifuged for 30 min at 7000*g* and the pellet resuspended in 50 mL of methotrexate column binding buffer (100 mM KCl, 50 mM K_2HPO_4, pH 7.0). The resulting sample was passed over a 25 mL methotrexate affinity column (*18*). The column was extensively washed (>5 column volumes of buffer) to remove unbound protein. DHFR was subsequently eluted in 5 mL fractions by passing a solution of 4 mM folic acid and 50 mM potassium phosphate, pH 8.0, over the column. SDS−PAGE was performed on fractions to determine which contained DHFR. The appropriate fractions were then pooled and dialyzed extensively against DEAE column buffer (50 mM K_2PO_4, pH 7.5) to remove folic acid from the solution. On the following day the sample was applied to a 120 mL DEAE ion-exchange column (GE Healthcare). All fractions were analyzed by SDS−PAGE. Fractions containing highly pure (>95%) DHFR were pooled, concentrated to 1 mg/mL, flash-frozen in liquid nitrogen, and stored at −80 °C.

Kinetic Analysis. Standard DHFR assays were conducted using a standard 1 cm path-length cuvette at 37 °C with continuous recording of change of OD at 340 nM. The assay contained 41 mM sodium phosphate buffer at pH 7.4, 8.9 mM 2-mercaptoethanol, 150 mM KCl, and saturating concentrations of NADPH and dihydrofolic acid (DHFA). With human DHFR, DHFA concentrations were 18 or 90 μM DHFA; 117 μM NADPH was used. The optimal level of DHFA for each protein was determined and selected to give maximal activity without approaching levels that might be inhibitory. Because K_i values take into account the amount of substrate in the assay, these differences do not affect the final value. Initial rates of enzyme activity were measured; rates were linear under standard conditions for about 5 min for human DHFR. Activity was linearly related to protein concentration under these conditions of assay.

K_m values were determined by holding either substrate or cofactor at a constant, saturating concentration and varying the other over a range of concentrations. The K_m value was determined by fitting the data to the Michaelis−Menten equation using nonlinear regression methods (Prism 4.0). The value of k_{cat} was determined from the V_{max} value and the protein concentration ($k_{cat} = V_{max}[E_{tot}]$) (Table 2).

K_i values were determined by measuring inhibition of the reaction at two or more concentrations of substrate (DHFA). For the competitive inhibitors such as trimethoprim, K_i could be calculated from the equation:

$$K_i = IC_{50}/(1 + S/K_m)$$

Methotrexate followed the pattern of a tight-binding inhibitor (*18*), and PY957 inhibition best fit a linear mixed model (*19*).

All determinations of IC_{50} were made by fitting percent inhibition data to a single site sigmoidal model with variable slope, using nonlinear regression methods (Prism 4.0). All inhibition curves required at least four points within the central segment of the sigmoidal curve. Statistical comparisons were preformed with InStat 2.03, using the nonparametric Welch *t* test because variances among groups could not be shown to be equal; this test is more conservative than the standard *t* test. These results are shown in Table 3. The values in the tables represent mean ± standard error of the mean when replicates are three or more; when $n = 1$ or 2, the values are the mean ±s standard error for the curve fitting. Additional graphical representations of these kinetic data are illustrated in Figures 1S and 2S of the Supporting Information.

Crystallization. Buffers for the Q35K single mutant protein and the Q35S/N64F and Q35S/N64S double mutant proteins of human DHFR were exchanged in a Centricon 10000 MWCO filter with 100 mM K_2HPO_4 buffer, pH 6.9, and concentrated to 4.2 mg/mL for the single mutant protein and 6.6 mg/mL for the double mutant proteins of hDHFR. The protein was incubated with NADPH and a 10:1 molar excess of the inhibitor, PY957, for 1 h over ice prior to crystallization using the hanging drop vapor diffusion method using siliconized glass coverslips. The 10 μL protein droplets that contained a final protein buffer of 100 mM K_2HPO_4, pH 6.9, with 30% saturated ammonium sulfate were suspended over a reservoir solution of 100 mM K_2HPO_4, pH 6.9, and 60% saturated ammonium sulfate with 3% (v/v) ethanol. Samples were stored at 14 °C, and crystals grew in about 3 days and were trigonal, space group *R*3 in the *H*3 hexagonal setting.

A data set for the single Q35K mutant protein hDHFR ternary complex was collected on a Rigaku RaxisIV imaging plate system with MaxFlux optics to 1.8 Å resolution, and a second, higher resolution data set was collected to 1.45 Å resolution using the remote access protocol on beam line 9-1 at the Stanford Synchrotron Radiation Laboratory (SSRL) facility (*20*−*22*). Only data from SSRL are reported for the single mutant. Data for the wild-type hDHFR ternary complex with PY957 and NADPH were also collected to 1.2 Å resolution on beam line 9-2 at SSRL. Data were collected on the Rigaku RaxisIV imaging plate system to 1.90−2.0 Å resolution for the two double mutants of the

Table 4: Data Collection and Refinement Statistics for the Wild-Type and Single and Double Mutant Proteins of Human DHFR NADPH Ternary PY957 Inhibitor Complexes

	Q35K-PY957	Q35S/N64S35S/N64F-PY957	Q35S/N64S35S/N64F-PY957	wt-PY957
		Data Collection		
PDB accession no.	3F8Y	3F87	3F91	3FS6
space group	*H*3	*H*3	*H*3	*H*3
cell dimensions (Å)				
$a = b$ (Å)	84.29	84.42	84.08	84.63
c (Å)	78.12	77.93	77.92	78.06
beamline	9-1 SSRL	RaxisIV	RaxisIV	9-2 SSRL
resolution (Å)	53.34−1.45 (1.53)	26.22−2.01 (2.2)	26.70−1.90 (2.0)	53.2−1.2
wavelength (Å)	1.00	1.5418	1.5418	1.00
R_{merge}	0.039	0.071	0.048	0.07
R_{sym} (%)[a,b]	0.046	0.081	0.055	0.02
completeness (%)[a]	99.1 (98.9)	97.0 (70.0)	99.5 (96.8)	100.0
observed reflections	153756	68430	79767	59797
unique reflections	50420	17593	20604	56766
$I/\sigma(I)$	16.7 (6.1)	16.3 (1.3)	28.1 (9.0)	20.8
multiplicity[a]	3.6 (3.0)	3.9 (1.7)	3.9 (1.7)	11.1
		Refinement and Model Quality		
resolution range (Å)	26.67−1.45	26.66−2.01	26.69−1.90	34.4−1.2
no. of reflections	34546	12666	15480	56766
R-factor [c]	19.0	16.1	18.5	24.5
R_{free}-factor [d]	22.8	21.9	24.2	26.0
total protein and ligand atoms	1957	1871	1753	1642
total water atoms	372	276	168	67
average *B*-factor (Å^2)	18.9	19.9	12.5	16.0
error in Luzzati plot	0.159	0.186	0.189	0.178
rms deviation from ideal				
bond lengths (Å)	0.010	0.018	0.016	0.009
bond angles (deg)	1.84	1.97	2.06	1.57
Ramachandran plot				
most favored regions (%)	90.6	94.3	92.5	91.2
additionally allowed regions (%)	9.4	5.0	6.9	8.8
generously allowed regions (%)	0.0	0.6	0.6	0.0
disallowed regions (%)	0.0	0.0	0.0	0.0

[a] The values in parentheses refer to data in the highest resolution shell. [b] $R_{sym} = \sum_h \sum_i |I_{h,i} - \langle I_h \rangle| / \sum_h \sum_i |I_{h,i}|$, where $\langle I_h \rangle$ is the mean intensity of a set of equivalent reflections. [c] *R*-factor $= \sum |F_o - F_c| / \sum F_o$, where F_o and F_c are observed and calculated structure factor amplitudes. [d] R_{free}-factor was calculated for *R*-factor for a random 5% subset of all reflections.

hDHFR ternary complex with NADPH and PY957. All data were processed using Mosflm (*23*). Diffraction statistics are shown in Table 4 for all complexes.

Structure Determination. The structures were solved by molecular replacement methods using the coordinates for wild-type human DHFR (1U72) (*24*) in the program Molref (*23*). Inspection of the resulting difference electron density maps was made using the program COOT (*25*) running on a Mac G5 workstation and revealed density for a ternary complex for all structures (Figure 2). To monitor the refinement, a random subset of all reflections was set aside for the calculation of R_{free} (5%). The model for the inhibitor was taken from the coordinates of the pcDHFR-NADPH-PY957 ternary complex (*16*). The parameter file for the cofactor and inhibitor was prepared using the Dundee PRODGR2 Server Web site (http://davapc1.bioch.dundee.ac.uk/programs/prodrg) (*26*). The final cycles of refinement were carried out using the program Refmac5 in the CCP4 suite of programs (*23*). The Ramachandran conformational parameters from the last cycle of refinement generated by PROCHECK (*27*) showed that more than 90% of the residues in all complexes have the most favored conformation and none are in the disallowed regions (Table 4). Coordinates for these structures have been deposited with the Protein Data Bank (accession numbers 3f8y, 3f87, 3f91, and 3fs6 for the hDHFR structures listed in Table 4).

RESULTS

Steady-State Kinetic Parameters. The parameters reported in Table 2 give the overall effect of mutations on catalytic activity. There is no significant departure from Michaelis−Menten kinetics observed for any of the variants. The K_m values for DHFA and NADPH for hDHFR (Table 2) are somewhat greater than previously reported values of 0.12 and 0.16 μM, respectively (*28*−*31*); however, our values were determined at 37 °C in the presence of 150 mM KCl, and the cited values were measured at 20 °C in the presence of NaCl, which likely accounts for the differences. The data in Table 2 show K_m values for DHFA are similar for pjDHFR, hDHFR, and its mutant proteins Q35S and Q35S/N64S. The mutant proteins Q35K, N64S, N64F, and Q35K/N64F all have lower K_m values for DHFA than either wild-type human or wild-type pcDHFR. The values of k_{cat} previously reported for hDHFR range from 6.9 to 11 s^{-1}, assayed at 20 °C (*28*−*31*), and are generally in line with the value of 40 s^{-1} we measured at 37 °C. The value of k_{cat} is not significantly affected by any of the mutations studied.

Inhibition of hDHFR Variants by Antifolates. The K_i for all variants at positions 35 and 64 were determined for TMP, MTX, and PY957 (Table 3). Mutant protein for N64S DHFR had a K_i value for MTX statistically significantly lower than that of hDHFR. Mutant proteins Q35S and Q35S/N64S hDHFR showed K_i values for MTX that were identical to

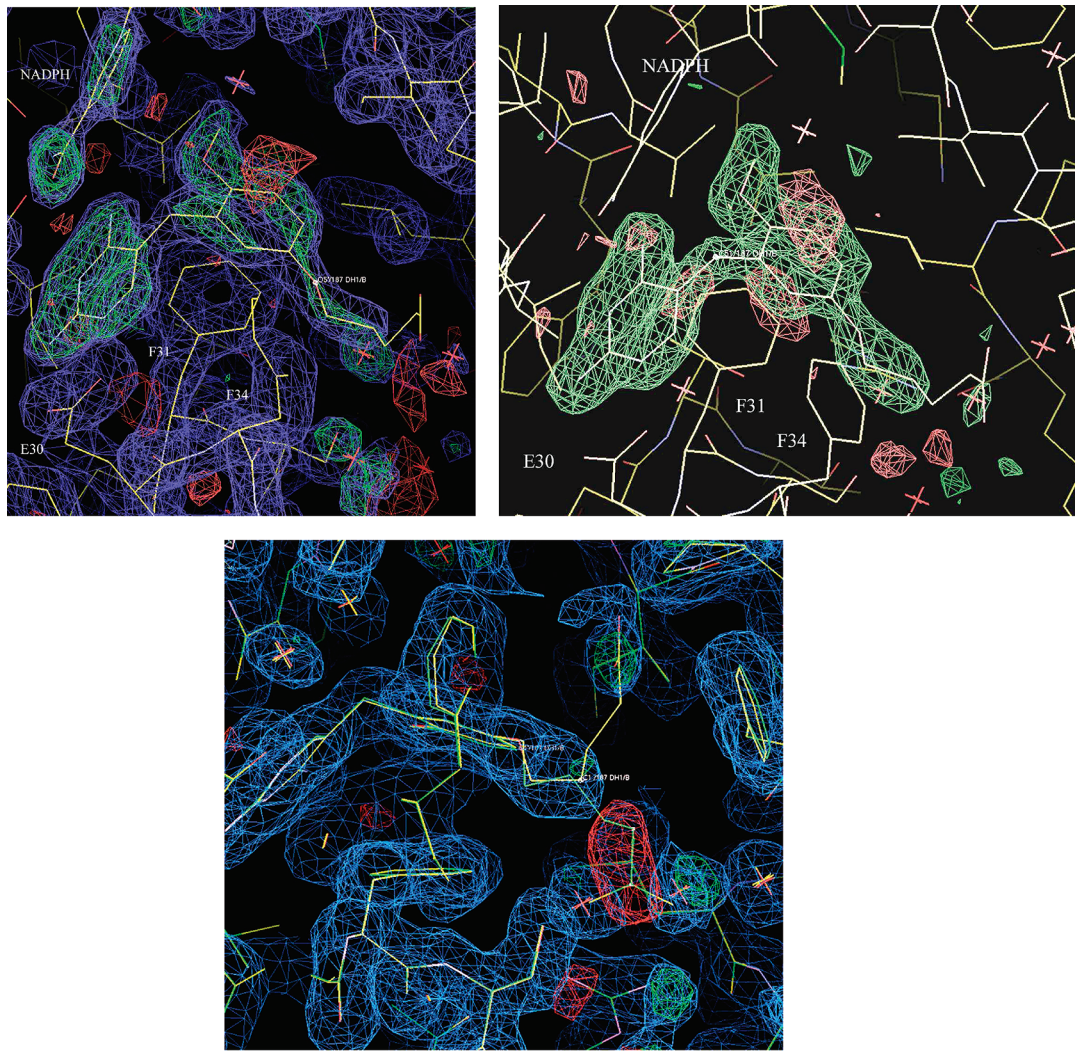

FIGURE 2: (Top left) $2F_o - F_c$ difference electron density map (0.8σ, blue; 3σ, green) showing the fit of the inhibitor PY957 and NADPH in the active site of the Q35S/N64F human DHFR ternary complex with NADPH and PY957. The map was phased using only the enzyme hDHFR as the search model. (Top right) Omit map from final refinement showing $F_o - F_c$ density for PY957 (3σ, green). (Bottom) $2F_o - F_c$ difference electron density map (0.8σ, blue) showing the fit of the inhibitor PY957 in the active site of the Q35S/N64F double mutant of the human DHFR ternary complex with NADPH and PY957. Model of PY957 (green) in expected conformation interacting with Arg70 reveals negative (−3σ, red) density indicating that the side chain does not fit in this position. The correct model (yellow) indicates that water molecules interact with Arg70 while the side chain is folded such that it is between Phe31 and Phe64.

the value for pjDHFR but were not statistically significantly lower than the K_i for hDHFR. In contrast, all mutant proteins converting hDHFR to a more pc-like active site (Q35K, N64F, Q35K/N64S) showed values near that of wild-type pcDHFR and were statistically lower than the value for hDHFR.

K_i values for TMP are in general agreement with the values reported from enzyme taken from AIDS patients (Table 3) (*5*). The K_i values for TMP were statistically significantly lower than the value for hDHFR in the Q35S, N64S, and Q35S/N64S mutant protein series but were not as low as the value for native pjDHFR. In contrast, hDHFR mutants Q35K, N64F, and Q35K/N64F showed K_i values that were statistically lower than the value for hDFHR but not significantly different than the value for pcDHFR. These results suggest that the selectivity of interaction of TMP with DHFR depends heavily on the residues at positions 35 and 64. However, structural data reported for the ternary complex of pcDHFR with NADPH and TMP indicate few interactions of TMP with Lys37 and Phe69 (*32*).

The K_i values for PY957 follow a pattern similar to that of TMP: mutant Q35S/N64S has a K_i value lower than hDHFR but higher than pjDHFR, and all K_i values for mutant hDHFR with pcDHFR substitutions (Q35K, N64F, Q35K/N64F) are significantly lower than the value for hDHFR but not significantly different from the K_i for pcDHFR. These results suggest that PY957 exploits some of the same interactions as TMP to achieve selectivity.

Overall Structure and Ligand Binding Conformation. The Q35S/N64S doubly substituted mutant protein hDHFR was designed to make the active site of the human enzyme more like the active site of pjDHFR while the single Q35K single mutant protein makes that position like that of the pcDHFR active site, whereas the Q35S/N64F double mutant protein is a cross between the pc- and pjDHFR sequences at these positions. Overall, the structures of these mutant proteins resemble those previously reported for hDHFR and preserve the previously reported hydrogen bond network involving structural water, the conserved residues Thr136, Trp24, Glu30, and the N1 nitrogen and 2-amino group of PY957 (*28*−*30*).

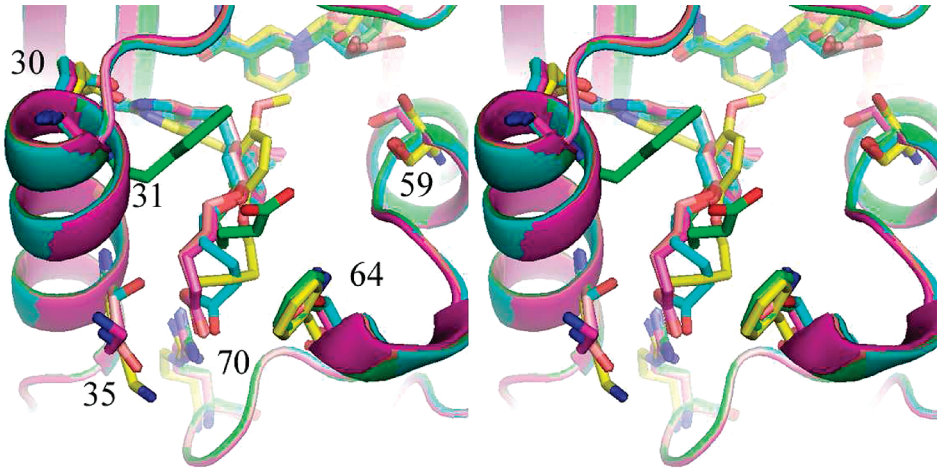

FIGURE 3: Stereoview of the superposition of the hDHFR-NADPH-PY957 ternary complexes with Q35K (violet), the Q35S/N64S double mutant (cyan), the Q35S/N64F double mutant (green), wild-type hDHFR (pink), and the pcDHFR wild type-NADPH-PY957 ternary complex (yellow) (*16*). The wild-type structure has nearly the same conformation as the single mutant protein. Figure was drawn with PyMol (*33*).

Similarly, the 4-amino group of PY957 maintains contact with the conserved residues Ile7 and Tyr121 and NADPH. The binding orientation of the diaminopyrimidine ring of PY957 is similar to that observed in the pcDHFR ternary structure (*16*).

The conformation of PY957 in the hDHFR wild-type and mutant protein complexes differs significantly from that observed in the pcDHFR ternary inhibitor complex (Figure 5) (*16*). Comparison of the torsion angle rotation about the C5−C51 and C51−C1′ bonds (Figure 1, Table 5) reveals that the two ring systems are mutually perpendicular, in contrast to that observed in the pcDHFR complex (*16*). This conformation of PY957 in the hDHFR mutant protein complexes positions the 2′-methoxy carbon such that it makes hydrophobic contact with the methyl carbon of Thr56 (3.0, 3.5, and 3.4 Å for the single Q35K and double Q35S/N64F and Q35S/N64S mutants, respectively), with the side chain of Val115 (4.1, 3.7, and 3.7 Å), and to the nicotinamide ring of NADPH (3.6, 4.0, and 3.8 Å). The 2′-methoxy oxygen makes contact with the backbone carbonyl of Val115 (3.4, 3.8, and 3.7 Å, respectively). In the pcDHFR complex with PY957 (*16*), these contacts are to Leu25 (4.0 Å), Thr61 (4.8 Å), and the nicotinamide ring (3.7 Å).

There are also significant differences in the conformation among the "(5′-ω-carboxyalkyoxy)" side chains of PY957 observed in all the variant complexes of hDHFR (Table 5 and Figure 3). In the Q35K structure that has Lys35 and Asn64 in the binding pocket, the methylene carbons of the side chain of PY957 are extended and make weak hydrophobic contacts to the Lys35 and Asn64 (3.9−4.8 Å). In the case of the Q35S/N64S double mutant, these residues are both Ser, and the side chain methylene carbons are folded such that they are closer to Leu60 and Ser59 (3.3−4.3 Å, respectively) (Figure 3). In the cross-species variant Q35S/N64F, the side chain conformation has changed significantly and is positioned between Phe31 and Phe64 rather than forming interactions with the conserved Arg70 as in the other mutant structures (Figure 4). The corresponding residue in pcDHFR is Phe69 (pcDHFR numbering), that can contribute strong hydrophobic interactions to the methylene carbons of the inhibitor side chain (*16*). Thus, although the two mutant hDHFR forms and pcDHFR differ in the way they interact

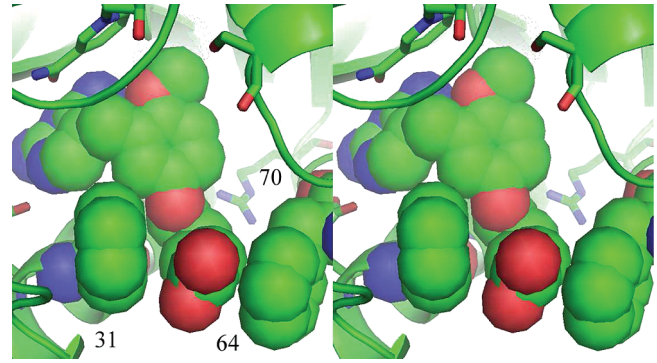

FIGURE 4: Stereoview of the interactions of the PY957 side chain in the active site of the double mutant protein Q35S/N64F of hDHFR illustrating the hydrophobic contacts made between Phe31 and Phe64 of the mutant protein and the methylene carbons of the PY957 side chain. This conformation has the side chain flipped such that the carboxylate oxygen atoms no longer interact with Arg70 as observed in the other PY957 structures.

with the methylene carbons in the side chain of PY957, the single Q35K and Q35S/N64S double mutants retain these interactions to some extent.

The position of the side chain of the conserved Arg70 is maintained by a network of hydrogen bond contacts from the side chains of residues Thr38 and Thr39 and from the backbone functional groups of Lys68 (*16*). As expected, the carboxylate group of PY957 forms close contacts to the conserved Arg70 in hDHFR Q35K and Q35S/N64S variant complexes; however, in the case of the Q35S/N64F double mutant, there is an unexpected change in the inhibitor side chain conformation such that it no longer makes contact with Arg70. In this complex, the inhibitor carboxylate interactions are replaced by water molecules (Figure 2c). The carboxylate oxygen atoms of PY957 in this alternate conformation make weak interactions with water molecules near the surface of the enzyme. The side chain may be disordered as the *B*-values for thermal motion for the methylene carbons of the side chain are nearly twice (about 30) those in the remaining structure.

In all the mutant protein DHFR structures, NADPH is fully occupied and is bound in an extended conformation similar to other DHFR cofactor complexes (*11*, *16*). In the case of

Table 5: Bridge Conformation for PY957 hDHFR Complexes[a]

torsion angle (deg)	hDHFR-Q35K-PY957	hDHFR-Q35S/N64S-PY957	hDHFR-Q35S/N64FPY957	pcDHFR-PY957	hDHFR-PY957
C4−C5−C51−C1′	−88.9	−80.7	−86.5	179.1	−88.7
C5−C51−C1′−C2′	97.2	96.5	100.3	−88.9	98.3
C51−C1′−C2′−O2′	−1.1	−1.4	−3.5	0.1	−1.4
C1′−C2′−O2′−C21	124.5	168.4	163.4	−115.8	140.5
C4′−C5′−O51−C52	78.5	85.0	−69.9	51.0	−101.5
C51′−O51−C52−C53	152.0	157.8	141.0	163.4	150.7
O51−C52−C53−C54	−154.1	−48.5	68.1	39.2	−142.6
C52−C53−C54−C55	141.1	−60.9	−112.7	63.6	140.9
C53−C54−C55−C56	−115.6	−64.7	159.9	49.8	−126.2
C54−C55−C56−O7	177.6	−77.9	−133.3	−118.1	176.2

[a] Numbering scheme is shown in Figure 1.

the wild-type hDHFR ternary complex, the cofactor is partially occupied in the extended conformation. The carboxamide group of the nicotinamide rings, which is syn to the nicotinamide ring N, makes a series of strong hydrogen bonds with the backbone carbonyls of the conserved residues Ile7 and Val115 in hDHFR. The conserved cis peptide linkage between the invariant Gly117 and Gly118 permits the pyrophosphate oxygen atoms of the cofactor to interact.

DISCUSSION

This is the first report of the kinetic and structural parameters for the pjDHFR and for the single and double variants at positions 35 and 64 of hDHFR that make the human enzyme resemble the DHFR from the two opportunistic pathogens from *Pneumocystis*, i.e., Q35K and N64F for human to pcDHFR and Q35S and N64S for human to pjDHFR. Structural data suggest that binding of PY957 is qualitatively different among pcDHFR, Q35S/N64F, Q35S/N64S hDHFR, and Q35K hDHFR. Likewise, the kinetic data show differences in K_i values for these three enzyme forms: Q35K hDHFR has the lowest K_i for PY957 (8.3 ± 0.4 nM), followed by pcDHFR (21.9 ± 9.3 nM) and Q35S/N64S hDHFR (66 ± 2 nM), and these values are statistically different from one another.

Converting key active site residues at positions 35 and 64 of the human DHFR to amino acids found at these analogous sites in *P. jirovecii* or *P. carinii* DHFR had little effect on k_{cat}. This result is rational, considering that selective pressure during evolution would be presumed to preserve catalytic activity of this important metabolic enzyme; however, the mutations at positions 35 and 64 of the human enzyme do show a small effect on the K_m for DHFA. The single and double mutants introducing *P. carinii* residues into the human enzyme at positions 35 and 64 show a statistically lower K_m for substrate DHFA than the native human enzyme; the same tendency is seen for the *P. jirovecii* residues, but the effect is not statistically significant.

Given that our steady-state conditions for determining K_m were with saturating concentrations of NADPH, the enzyme reaction scheme simplifies to

$$E + S \underset{k_{-1}}{\overset{k_1}{\leftrightarrow}} ES \xrightarrow{k_{cat}} E + P$$

and thus K_m is defined as $(k_{-1} + k_{cat})/k_1$. Our determinations of k_{cat} show it to be unchanged in the mutants studied. Therefore, lowered K_m values must reflect either a decreased k_{-1} value or an increased k_1 value or both; in either case, the suggestion is that these mutations affect affinity of the substrate for the active site. Therefore, if we use an array of substrate analogues to probe the active sites of native and mutant forms of DHFR, we would expect to see significant differences in K_i, the equilibrium dissociation constant for binding (k_{-1}/k_1).

For the competitive inhibitor TMP, our results agree with the above prediction, in that we saw improved affinity for TMP (lower K_i) in all mutants. For the series of mutants converting human to *P. jirovecii*-like residues at positions 35 and 64, the changes in K_i values relative to those of native human enzyme were as follows: Q35S, 2.89-fold reduction; N64S, 30.59-fold reduction; Q35SN64S, 4.33-fold reduction. Using the reasoning suggested by Mildvan (*14*), these values may be converted to log form: Q35S, $10^{0.46}$; N64S, $10^{1.49}$; Q35SN64S, $10^{0.64}$. The effects of the two residues are clearly not additive (i.e., $10^{1.95} \neq 10^{0.64}$), suggesting that the residues do not act independently in affecting TMP binding. For mutant proteins converting hDHFR to a more *P. carinii*-like active site, the log values of changes are as follows: Q35K, $10^{1.12}$; N64F, $10^{1.03}$; Q35K/N64F, $10^{0.9}$. The mutations Q35S and N64S are neither additive nor synergistic, but rather the presence of Q35S seems capable of reversing the effects of N64S; reversal of the effects on K_i is complete or nearly complete for MTX and TMP but only partial for PY957. Similar analysis based on the K_i values for the pseudoirreversible inhibitor MTX and the linear mixed inhibitor PY957 also suggests a degree of antagonism in both sets of mutants; i.e., the effect on the double mutant is less than the effect seen for one or both of the single mutants.

These data are consistent with the structural results observed for the single and double mutants bound with PY957. In these structures, variations in the side chain conformation reflect differences in its interactions with the mutants at positions 35 and 64 in the hDHFR ternary complexes with PY957 while maintaining the strong interactions of the inhibitor carboxylate with Arg70. The conformation of the PY957 side chain in the Q35S/N64F double mutant protein complex was unexpected as the side chain of PY957 flips away from Arg70 and instead the methylene carbons of the side chain form hydrophobic interactions with Phe31 and Phe64 (Figure 4). The carboxylate oxygen atoms of PY957 in this orientation make weak interactions with water molecules on the surface of the enzyme.

Structural data for the binding of PY957 to the hDHFR variants and to pcDHFR provide insight into the contribution of the active site residues at positions 35 and 64 to the selectivity and specificity of inhibitor binding to h-, pc-, and pjDHFR. These data show that the conformation of the "5-

ω-carboxyalkyoxyl" side chain of PY957 is flexible and can adopt conformations that optimize its binding interactions with the residues that line the active site. These data suggest that the interactions with side chains of residues at position 64 may contribute more to inhibition than those at position 35 as indicated by the alternative side chain conformation observed in the structure of the Q35S/N64F double mutant of hDHFR. These results imply that the hydrophobic contributions to binding by contacts to Phe31 and Phe64 by the PY957 side chain are greater than those made by the interactions of Ile33 and Phe69 in the pcDHFR ternary complex with PY957 (*16*). Since Ile33 is smaller than Phe31, it cannot make the same contribution to hydrophobic binding as observed in the Q35S/N64F human complex. Although the PY957 side chain can interact electrostatically with Arg75 in the pcDHFR ternary complex, the side chain conformation changes to enhance its hydrophobic interactions with Phe69 and may result in the twisting of the torsion angle between the two ring systems of PY957 as a consequence of this interaction.

The relationships between specificity of PY957 inhibitory potency and active site mutations in hDHFR correlate with the conformational patterns observed in PY957 binding and the enhanced binding observed for those variants that make these active site positions more like those of the *Pneumocystis* DHFR enzymes.

These results taken together suggest that PY957 interacts with the DHFR enzymes from *Pneumocystis* in ways that are different from TMP such that binding is enhanced (lower K_i) and selectivity is still achieved. This conclusion is supported by the observation that TMP binding follows the pattern of classical competitive inhibition (only K_m affected), whereas PY957 best fits a model of linear mixed inhibition (both K_m and V_{max} affected).

These data validate the hypothesis that the increased selectivity of PY957 for pcDHFR is in part due to contributions of the species-specific residues Lys37 and Phe69 of pcDHFR. This insight into the contribution of species-specific residues to inhibitor binding will help in the design of more selective inhibitors that target specific opportunistic fungal pathogens.

ACKNOWLEDGMENT

The authors thank the beam line staff at SSRL for their support. Portions of this research were carried out at the Stanford Synchrotron Radiation Laboratory, a national user facility operated by Stanford University on behalf of the U.S. Department of Energy, Office of Basic Energy Sciences. The SSRL Structural Molecular Biology Program is supported by the Department of Energy, Office of Biological and Environmental Research, and by the National Institutes of Health, National Center for Research Resources, Biomedical Technology Program, and the National Institute of General Medical Sciences. The authors also thank Dr. Edward Snell for help in data collection and processing.

SUPPORTING INFORMATION AVAILABLE

Figure S1, illustration of the dose−response curve for PY957 with the N64F mutant protein of hDHFR, and Figure S2, graphical illustration of the effect of hDHFR active site mutations on K_i values for the inhibitor PY957. This material is available free of charge via the Internet at http://pubs.acs.org.

REFERENCES

1. Kovacs, J. A., Gill, V. J., Meshnick, S., and Masur, H. (2001) New Insights into Transmission, Diagnosis, and Drug Treatment of *Pneumocystis carinii* Pneumonia. *J. Am. Med. Assoc. 286*, 2450–2460.
2. Hughes, W. T. (1991) Prevention and Treatment of *Pneumocystis carinii* Pneumonia. *Annu. Rev. Med. 42*, 287–295.
3. Totet, A., Duwat, H., Magois, E., Jounieaux, V., Roux, P., Raccurt, C., and Nevez, G. (2004) Similar Genotypes of *Pneumocystis jirovecii* in Different Forms of *Pneumocystis* Infection. *Microbiology 150*, 1173–1178.
4. Benfield, T., Atzori, C., Miller, R. F., and Helweg-Larsen, J. (2008) Second-Line Salvage Treatment of AIDS-Associated *Pneumocystsis jirovecii* Pneumonia. *J. Acquired Immune Defic. Syndr. 48*, 63–67.
5. Ma, L., and Kovacs, J. A. (2000) Expression and Characterization of Recombinant Human-derived *Pneumocystis carinii* Dihydrofolate Reductase. *Antimicrob. Agents Chemother. 44*, 3092–3096.
6. Nahimana, A., Rabodonirina, M., Bille, J., Francioli, P., and Hauser, P. M. (2004) Mutations of *Pneumocystis jirovecii* Dihydrofolate Reductase Associated with Failure of Prophylaxis. *Antimicrob. Agents Chemother. 48*, 4301–4305.
7. Chan, D. C. M., and Anderson, A. C. (2006) Towards Species-Specific Antifolates. *Curr. Med. Chem. 13*, 377–398.
8. Gangjee, A., Jain, H., and Kurup, S. (2007) Recent Advances in Classical and Non-classical Antifolates as Antitumor and Antiopportunistic Infection Agents, Part I. *Anticancer Agents Med. Chem. 7*, 523–542.
9. Gangjee, A., Jain, H., and Kurup, S. (2008) Recent Advances in Classical and Nonclassical Antifolates as Antitumor and Antiopportunistic Infection Agents, Part II. *Anticancer Agents Med. Chem. 8*, 205–231.
10. Gangjee, A., Kurup, S., and Namjoshi, O. (2007) Dihydrofolate Reductase as a Target for Chemotherapy in Parasites. *Curr. Pharm. Des. 13*, 609–639.
11. Cody, V., and Schwalbe, C. H. (2006) Structural Characteristics of Antifolate Dihydrofolate Reductase Enzyme Interactions. *Crystallogr. Rev. 12*, 301–333.
12. Volpato, J. P., Fossati, E., and Pelletier, J. N. (2007) Increasing Methotrexate Resistance by Combination of Active-site Mutations in Human Dihydrofolate Reductase. *J. Mol. Biol. 373*, 599–611.
13. Fossati, E., Volpato, J. P., Poulin, L., Guerrero, V., Dugas, D.-A., and Pelletier, J. N. (2008) 2-Tier Bacterial and In Vitro Selection of Active and Methotrexate-Resistant Variants of Human Dihydrofolate Reductase. *J. Biomol. Screen. 13*, 504–514.
14. Mildvan, A. S. (2004) Inverse Thinking about Double Mutants of Enzymes. *Biochemistry 43*, 14517–145120.
15. Rosowsky, A., Forsch, R. A., and Queener, S. F. (2003) Further Studies on 2,4-Diamino-5-(2′,5′-disubstituted benzyl)pyrimidines as Potent and Selective Inhibitors of Dihydrofolate Reductases from Three Major Opportunistic Pathogens of AIDS. *J. Med. Chem. 46*, 1726–1736.
16. Cody, V., Pace, J., Chisum, K., and Rosowsky, A. (2006) New Insights into DHFR Interactions: Analysis of *Pneumocystis carinii* and Mouse DHFR Complexes with NADPH and Two Highly Potent 5-(ω-Carboxy(alkyloxy)) Trimethoprim Derivatives Reveals Conformational Correlations with Activity and Novel Parallel Ring Stacking Interactions. *Proteins: Struct., Funct., Bioinf. 65*, 959–969.
17. Mossessova, E., and Lima, C. D. (2000) Ulp1-SUMO Crystal Structure and Genetic Analysis Reveal Conserved Interactions and a Regulatory Element Essential for Cell Growth in Yeast. *Mol. Cell 5*, 865–876.
18. Appleman, J. R., Prendergast, N., Delcamp, T. J., Freisheim, J. H., and Blakley, R. L. (1988) Kinetics of the Formation and Isomerization of Methotrexate Complexes of Recombinant Human Dihydrofolate Reductase. *J. Biol. Chem. 263*, 10304–10313.
19. Segel, I. H. (1975) *Enzyme Kinetics: Behavior and Analysis of Rapid Equilibrium and Steady-State Enzyme Systems*, 957 pp, Wiley-Interscience, New York.
20. McPhillips, T. M., McPhillips, S. E., Chiu, H. J., Cohen, A. E., Deacon, A. M., Ellis, P. J., Garman, E., Gonzalez, A., Sauter, N. K., Phizackerley, R. P., Soltis, S. M., and Kuhn, P. (2002) Blu-Ice and the Distributed Control System: Software for Data Acquisition

and Instrument Control at Macromolecular Crystallography Beamlines. *J. Synchrotron Radiat. 9*, 401–406.
21. Cohen, A. E., Ellis, P. J., Miller, M. D., Deacon, A. M., and Phizackerley, R. P. (2002) An Automated System to Mount Cryocooled Protein Crystals on a Synchrotron Beamline, Using Compact Sample Cassettes and a Small-scale Robot. *J. Appl. Crystallogr. 35*, 720–726.
22. Gonzalez, A., Moorhead, P., McPhillips, S. E., Song, J., Sharp, K., Taylor, J. R., Adams, P. D., Sauter, N. K., and Soltis, S. M. (2008) Web-Ice: Integrated Data Collection and Analysis for Macromolecular Crystallography. *J. Appl. Crystallogr. 41*, 176–184.
23. Collaborative Computational Project, No. 4 (1994) The CCP4 Suite: Programs for Protein Crystallography. *Acta Crystallogr. D50*, 760–763.
24. Cody, V., Luft, J. R., and Pangborn, W. (2005) Understanding the Role of Leu22 Variants in Methotrexate Resistance: Comparison of Wild-type and Leu22Arg Variant Mouse and Human Dihydrofolate Reductase Ternary Crystal Complexes with Methotrexate and NADPH. *Acta Crystallogr. D61*, 147–155.
25. Emsley, P., and Cowtan, K. (2004) Coot: Model-Building Tools for Molecular Graphics. *Acta Crystallogr. D60*, 2126–2132.
26. Schuettelkopf, A. W., and van Aalten, D. M. F. (2004) PRODRG: A Model Tool for High-throughput Crystallography of Protein-ligand Complexes. *Acta Crystallogr. D60*, 1355–1363.
27. Laskowski, R. A., MacArthur, M. W., Moss, D. S., and Thornton, J. M. (1993) PROCHECK: A Program to Check the Stereochemical Quality of Protein Structure. *J. Appl. Crystallogr. 26*, 283–291.
28. Chunduru, S. K., Cody, V., Luft, J. R., Pangborn, W., Appleman, J. R., and Blakley, R. L. (1994) Methotrexate-resistant Variants of Human Dihydrofolate Reductase: Effects of Phe31 Substitutions. *J. Biol. Chem. 269*, 9547–9555.
29. Lewis, W. S., Cody, V., Galitsky, N., Luft, J. R., Pangborn, W., Chunduru, S. K., Spencer, H. T., Appleman, J. R., and Blakley, R. L. (1995) Methotrexate-resistant Variants of Human Dihydrofolate Reductase with Substitutions of Leucine 22: Kinetics, Crystallography and Potential as Selectable Markers. *J. Biol. Chem. 270*, 5057–5064.
30. Cody, V., Luft, J. R., Pangborn, W., and Gangjee, A. (2003) Analysis of Three Crystal Structure Determinations of a 5-Methyl-6-N-Methylanalino Pyridopyrimidine Antifolate Complex with Human Dihydrofolate Reductase. *Acta Crystallogr. D59*, 1603–1609.
31. Appleman, J. R., Beard, W. A., Delcamp, T. J., Prendergast, N. J., Freisheim, J. H., and Blakley, R. L. (1990) Unusual Transient- and Steady-state Kinetic Behavior is Predicted by the Kinetic Scheme Operational for Recombinant Human Dihydrofolate Reductase. *J. Biol. Chem. 265*, 2740–2748.
32. Champness, J. N., Achari, A., Ballantine, S. P., Bryant, P. K., Delves, C. J., and Stammers, D. K. (1994) The Structure of *Pneumocystis carinii* Dihydrofolate Reductase to 1.9Å Resolution. *Structure 2*, 915–924.
33. DeLano Scientific LLC, PyMol.

BI801960H